

Article

The Effects of Zr-doping into Ceria for the Dry Reforming of Methane over Ni/CeZrO₂ catalysts: In-situ Studies with XRD, XAFS and AP-XPS

Feng Zhang, Zongyuan Liu, Xiaobo Chen, Ning Rui, Luis E. Betancourt, Lili Lin, Wenqian Xu, Cheng-Jun Sun, A. M. Milinda Abeykoon, Jose A. Rodriguez, Kristijan Lorber, Janvit Teržan, Petar Djinovic, and Sanjaya D. Senanayake

ACS Catal., **Just Accepted Manuscript** • DOI: 10.1021/acscatal.9b04451 • Publication Date (Web): 06 Jan 2020

Downloaded from pubs.acs.org on January 15, 2020

Just Accepted

"Just Accepted" manuscripts have been peer-reviewed and accepted for publication. They are posted online prior to technical editing, formatting for publication and author proofing. The American Chemical Society provides "Just Accepted" as a service to the research community to expedite the dissemination of scientific material as soon as possible after acceptance. "Just Accepted" manuscripts appear in full in PDF format accompanied by an HTML abstract. "Just Accepted" manuscripts have been fully peer reviewed, but should not be considered the official version of record. They are citable by the Digital Object Identifier (DOI®). "Just Accepted" is an optional service offered to authors. Therefore, the "Just Accepted" Web site may not include all articles that will be published in the journal. After a manuscript is technically edited and formatted, it will be removed from the "Just Accepted" Web site and published as an ASAP article. Note that technical editing may introduce minor changes to the manuscript text and/or graphics which could affect content, and all legal disclaimers and ethical guidelines that apply to the journal pertain. ACS cannot be held responsible for errors or consequences arising from the use of information contained in these "Just Accepted" manuscripts.

The Effects of Zr-doping into Ceria for the Dry Reforming of Methane over Ni/CeZrO₂ Catalysts: *In-situ* Studies with XRD, XAFS and AP-XPS

Feng Zhang,¹ Zongyuan Liu,² Xiaobo Chen,³ Ning Rui,² Luis E. Betancourt,² Lili, Lin,² Wenqian Xu,⁴ Chengjun Sun,⁴ A. M. Milinda Abeykoon,⁵ José A. Rodriguez,^{1,2} Janvit Teržan,⁶ Kristijan Lorber,⁶ Petar Djinović^{6*} and Sanjaya D. Senanayake^{2*}

¹ Materials Science and Chemical Engineering Department, Stony Brook University, Stony Brook, NY 11794, USA

² Chemistry Division, Brookhaven National Laboratory, Upton, NY 11973, USA

³ Program of Materials Science and Engineering, Department of Mechanical Engineering, State University of New York at Binghamton, NY 13902, USA.

⁴ X-ray Science Division, Advanced Photon Source, Argonne National Laboratory, Lemont, IL 60439, USA

⁵ Photon Science Division, National Synchrotron Light Source II, Upton, 11973 NY, USA

⁶ Department of Inorganic Chemistry and Technology, National Institute of Chemistry, Hajdrihova 19, SI-1001 Ljubljana, Slovenia

Corresponding Authors: Petar Djinović [petar.djinovic@ki.si], Sanjaya D. Senanayake [ssenanay@bnl.gov]

ABSTRACT

The methane activation and methane dry reforming reactions were studied and compared over 4 wt% Ni/CeO₂ and 4 wt% Ni/CeZrO₂ (containing 20 wt% Zr) catalysts. Upon the incorporation of Zr into the ceria support, the catalyst exhibited a significantly improved activity and H₂ selectivity. To understand the effects of the Zr dopant on Ni and CeO₂ during the DRM reaction and to probe the structure–reactivity relationship underlying the enhanced catalytic performance of the mixed-oxide system, *in-situ* Time Resolved X-ray diffraction (TR-XRD), X-ray absorption fine structure (XAFS) and ambient-pressure X-ray photoelectron spectroscopy (AP-XPS) were employed to characterize the catalysts under the reaction conditions. The TR-XRD and AP-XPS indicate ceria-zirconia supported Ni (Ni/CeZrO₂) is of higher reducibility than the pure ceria supported Ni/CeO₂ upon the reaction with pure CH₄ or for the methane dry reforming reaction. The active state of the Ni/CeZrO₂ under optimum DRM conditions (700 °C) was identified as Ni⁰, Ce³⁺/Ce⁴⁺ and Zr⁴⁺. The particle size of both nickel and the ceria support under the reaction conditions were analyzed by Rietveld refinement and EXAFS fitting. The Zr in the ceria support prevents particle sintering and maintains small particle sizes for both metallic nickel and the partially reduced ceria support under reaction conditions, through a stronger metal-support interaction. Additionally, Zr prevents Ni migration from the surface into ceria forming a Ce_{1-x}Ni_xO_{2-y} solid solution, which is seen in Ni/CeO₂, thus helps to preserve the active Ni⁰ on the Ni/CeZrO₂ surface.

KEYWORDS: nickel, ceria, zirconia, CeZrO₂ solid solution, XRD, XAFS, AP-XPS, dry reforming of methane

1. INTRODUCTION

The ability to simultaneously activate, then convert both CH₄ and CO₂ into useful intermediates or products through a catalytic process offers viable solutions for sustainable commercial fuel processing, and a practical solution to the irreversible and harmful impact of global greenhouse gas emissions.¹⁻⁴ Often, both CH₄ and CO₂ are found together in fossil fuels, bio fuels or land fill sources and there is a steep energy cost for the sequestration, separation and conversion of purified components prior to processing.⁵⁻⁶ The catalytic Dry Reforming of Methane reaction (DRM: CH₄ + CO₂ ↔ 2CO + 2H₂), is one way in which the direct production of synthesis gas (CO + H₂) can be obtained from both chemically robust reactants without the need of additional steps in conversion.

Our recent work has highlighted the metal-oxide interface and interactions in supported and inverse catalysts as key factors for achieving new pathways for activating CH₄ and CO₂ simultaneously at low temperatures.⁷⁻¹⁰ Our primary focus has been on the M-CeO₂ class of catalysts, including M = Co, Ni, Fe, Cu, Ru in intimate contact with the surfaces of ceria supports. Our observations have shown that the chemical role of the metal can be distinct, while a special relationship between the metal and support at low coverages, with high dispersion occurs with the reduced Ce³⁺ rich surfaces that can achieve catalytic chemistry not possible with bulk metals or pure oxide surfaces. This concept is supported by previous studies demonstrating the important role of the ceria support to anchor and then activate metals with high chemical potential.¹¹

In this work we have extended the study to the modification of the ceria support, to explore if similar chemistry is observed for the M-Ceria interaction, in the presence of a commonly used dopant such as Zr. It has been extensively reported that by introducing dopants such as Zr, La or W into ceria, the oxygen storage capacity and reducibility of the ceria support could be enhanced.¹²⁻¹⁵ Previous studies also found increased catalytic activity for CO and CO₂ methanation, selective oxidation of ethanol and also DRM reaction when metal was supported on a CeO₂-ZrO₂ mixed oxide rather than on pure ceria.¹⁶⁻²¹ However, the origin behind the improved DRM reaction activity and the chemical/structural behaviors of both metal, Zr dopant and ceria support under challenging DRM reaction conditions has not been completely elucidated.

The ability to enhance the propensity for dry reforming chemistry is limited by our fundamental knowledge of the nature of catalyst surfaces and direct evidence for transformations that occur under difficult reaction conditions. Such an understanding requires observations of the process as they are taking place or '*in-situ*' using multiple probes of the catalyst, including the chemical, electronic and structural active state of the material ideally in similar reaction conditions. An added complication for the DRM process is the need for high temperatures ($> 400\text{ }^{\circ}\text{C}$) for sustained turnover, necessitating characterization at challenging temperature limits, often unachievable in many *in-situ* analytical techniques. In this study we utilize several commonly used techniques including XRD, XAFS and XPS but under elevated temperature and *in-situ* DRM conditions. We aim to unravel the reasons for improved DRM reaction performance with Zr dopants and establish a detailed autopsy of chemical and structural properties and role of Ni and Ce with and without Zr dopants as the DRM reaction proceeds.

2. EXPERIMENTAL

2.1. Catalyst synthesis. During the synthesis of the CeZrO_2 mixed oxide (containing around 20 wt% of Zr, and Ce:Zr atomic ratio is 3:1), 1.09 g of $\text{ZrO}(\text{NO}_3)_2 \cdot 6\text{H}_2\text{O}$ was dissolved in 5 ml of ultrapure water during sonication. After dissolution, 4.04 g of $\text{Ce}(\text{NO}_3)_3 \cdot 6\text{H}_2\text{O}$ was added and mixed until complete dissolution. Afterwards, 5 ml of propionic acid and 154 ml of ethylene glycol were added, and the solution was mixed for an additional 15 min, transferred to Teflon[®] clad stainless-steel autoclaves and treated at $180\text{ }^{\circ}\text{C}$ for 200 min. The autoclaves were quench cooled, the slurry centrifuged and calcined in air for 4 h at $450\text{ }^{\circ}\text{C}$. Synthesis of pure CeO_2 and ZrO_2 followed the same protocol as above, whereas only their individual precursor was used.

The 4 wt% nickel was deposited by slow addition of NH_4OH to the aqueous CeO_2 or CeZrO_2 suspension containing an appropriate amount of dissolved $\text{Ni}(\text{NO}_3)_2$. The pH of the suspension was raised to 9.5 over the course of 2 h, and the suspension was centrifuged, dried overnight at $70\text{ }^{\circ}\text{C}$ and calcined in air for 4 h at $450\text{ }^{\circ}\text{C}$.

2.2. Catalytic performance tests. The DRM catalytic performance of 4 wt% Ni/ CeO_2 and 4 wt% Ni/ CeZrO_2 catalysts were compared through the conversion, reaction rate and selectivity. A 10 mg powder catalyst diluted with a ~ 30 mg pre-calcined quartz ($900\text{ }^{\circ}\text{C}$) were loaded into a quartz tube and mounted on a plug flow reactor system. The catalysts were pre-reduced in 25 cc/min H_2 and 25 cc/min He mixture at $450\text{ }^{\circ}\text{C}$ for 30 min before switching to the DRM reaction gas mixture (10 cc/min CH_4 , 10 cc/min CO_2 and 30 cc/min N_2) at room temperature (weight

hourly space velocity: 300,000 ml/g_{cat}/h). The catalysts were then heated stepwise from room temperature to 700 °C with isothermal steps at 200, 300, 400, 500, 600, and 700 °C for 1 hour. The residual gas products were analyzed by a gas chromatography instrument (Agilent 7890A) equipped with flame ionization and thermal conductivity detectors, and the conversions, reaction rates were calculated employing the equations S1-S5. The H₂ selectivity was defined as the amount of H₂ produced with respect to the total H₂ and H₂O production (Equation S6).

2.3. Characterizations

2.3.1. Pair Distribution Function (PDF) and XRD. The PDF spectra of Ni/CeO₂ and Ni/CeZrO₂ samples, along with calcined CeO₂, ZrO₂ and NiO standards were collected at 28ID ($\lambda = 0.1667 \text{ \AA}$) of National Synchrotron Light Source (NSLS-II) of Brookhaven national Laboratory (BNL). The sample was loaded into a 1 mm OD, and 0.9 mm ID Kapton tube for the measurement, and PDFget3 was used to process the results.²² The *ex-situ* and *in-situ* time-resolved XRD analyses were carried out at 17BM ($\lambda = 0.24108 \text{ \AA}$) of the Advanced Photon Source (APS), at Argonne National Laboratory (ANL). A Clausen cell flow reactor was used for the *in-situ* methane activation and methane dry reforming measurement.²³ For the methane activation study, a gas mixture of 5 cc/min CH₄ and 5 cc/min He was introduced to around 2 mg of catalyst in the flow cell, and the sample was heated from room temperature to 700 °C with a 5 °C/min ramping rate under the methane atmosphere. For the dry reforming reaction, the sample (~2 mg) was pre-reduced under 5 cc/min H₂ and 5 cc/min He at 450 °C for 30 min, and a 2 cc/min CH₄, 2 cc/min CO₂ and 6 cc/min He gas mixture was used afterwards for the DRM reaction. The catalysts were heated stepwise from room temperature to 700 °C with a 10 °C/min ramping rate and 1-hour soak time at 200, 300, 400, 500, 600, and 700 °C temperature stages. An amorphous Si flat panel (Perkin Elmer) detector was used to collect two-dimensional XRD images throughout the reaction processes, and the images were subsequently processed with GSAS-II to obtain diagrams of Intensity versus 2θ . Rietveld analyses were also performed through GSAS-II to obtain information such as lattice parameter and crystallite size.²⁴

2.3.2. Transmission electron microscopy (TEM) and energy-dispersive X-ray spectroscopy (EDS). TEM, HAADF-STEM (high-angle annular dark field scanning transmission electron microscopy) and EDS element mapping were performed using a high-resolution analytical scanning/transmission electron microscope (S/TEM, FEI Talos F200X) operating at 200 keV at

the Center for Functional Nanomaterials (CFN) of Brookhaven National Laboratory (BNL). The post-reaction catalysts were collected immediately after it was cooled down from the DRM reaction condition at 700 °C to room temperature, and then dispersed in methanol by sonication. A droplet of suspension was introduced onto Holey-Carbon coated Cu grids and allowed to dry before imaging. The elemental mappings (Ni K-edge, Ce L-edge, Zr L-edge) were acquired with a four-quadrant 0.9-sr energy dispersive X-ray spectrometer (Super EDS).

2.3.3. XAFS. In-situ X-ray absorption near edge structure and (XANES) and extend X-ray absorption fine structure (EXAFS) during the DRM reaction on Ni/CeO₂ and Ni/CeZrO₂ were collected at the 20ID beamline of the Advanced Photon Source (APS), at Argonne National Laboratory (ANL). Approximately 2 mg samples were loaded into a Clausen cell and mounted in line with a gas flow system. The reaction conditions including the gas flow rate and the temperature profile were kept the same as the in-situ XRD measurements (2.3.1) for pre-treatment and for the DRM reaction. The Ni K-edge data was collected using fluorescence yield by a four-channel Vortex detector. At each temperature stage, three parallel spectra were collected and averaged together to improve the quality of the data. Data processing was performed using the IFEFFIT package and Nickel foil was used as the standard reference for the EXAFS fitting.²⁵

2.3.4. AP-XPS. A commercial SPECS AP-XPS chamber equipped with a PHOIBOS 150 EP MCD-9 analyzer at the Chemistry Division of Brookhaven National Laboratory (BNL) was used for AP-XPS analysis (Mg K α anode; 30 eV pass energy; 0.1 eV step size and energy resolution ~0.4 eV).²⁶ The powder catalyst was pressed onto an aluminum plate and loaded into the AP-XPS chamber. During the CH₄ activation process, 30 mTorr of CH₄ was introduced into the analysis chamber, and Ni 1s, Ce 3d and Zr 3d spectra were collected at 25, 200, 300, 400, and 500 °C. For the DRM reaction measurements, 20 mTorr of H₂ were used to pretreat the samples at 450 °C for 30 min in the analysis chamber. After evacuation of the H₂, a gas mixture of 30 mTorr CH₄ and 30 mTorr CO₂ was introduced into the analysis chamber, and the Ni 1s, Ce 3d and Zr 3d spectra were collected at 25, 200, 300, 400 and 500 °C under reaction conditions. The Ce 3d photoemission line with the strongest Ce⁴⁺ feature (916.9 eV) was used for the energy calibration of Ni 1s and Ce 3d peaks and C 1s (at 284.6 eV) was used for the energy calibration of Zr 3d spectra.

3. RESULTS AND DISCUSSION

3.1. Structural and morphological properties of the Ni/CeZrO₂ and Ni/CeO₂ catalysts.

Figure 1a shows the XRD patterns of the Ni/CeZrO₂ and Ni/CeO₂ samples as well as ZrO₂ and CeO₂ references. The green dashed line in the figure designates the position of the CeO₂ (111) diffraction peak and it demonstrates a broader CeO₂ (111) peak, shifted to a higher 2 theta value in the Ni/CeZrO₂ sample. The shift of the ceria peaks comes from the substitution of the smaller Zr⁴⁺ (0.8 Å) ions into Ce⁴⁺ sites (1.0 Å), and the consequent lattice contraction (~ 0.07 Å) induced by Zr dopants. The absence of ZrO₂ diffraction peaks, the broadness and shift of CeO₂ peaks, evident in the XRD pattern of Ni/CeZrO₂ suggests the formation of a CeZrO₂ solid solution which adopts a simple ceria cubic fluorite structure²⁷⁻³⁰. The blue arrows (see also the insets in Figure 1a for the enlarged area) in the figure denote the presence of crystalline NiO in both Ni/CeZrO₂ and Ni/CeO₂ samples. The first and second shell PDF spectra of Ni/CeO₂ and Ni/CeZrO₂ samples with ZrO₂, CeO₂ standards are provided in Figure 1b (See Figure S1 for the PDF spectra in long-range order). The mean bond lengths of the Ce-O pairs in the first shell of Ni/CeO₂ sample was the same as that in the CeO₂ standard, while in the Ni/CeZrO₂ sample, besides the Ce-O pairs at 2.35 Å, a shoulder at 2.13 Å was observed, which reflects the existence of Zr-O bonds. As for the second neighbor, the Ce-Ce pairs in Ni/CeO₂ sample and CeO₂ standard at 3.83 Å shifted to 3.79 Å in the Ni/CeZrO₂ sample, and there is no Zr-Zr feature shown in the Ni/CeZrO₂ sample. The peak shift is also consistent with the previous study by Milen Gateshki et al.,³¹ which confirms the formation of a homogeneous CeZrO₂ solid solution in our Ni/CeZrO₂ sample.

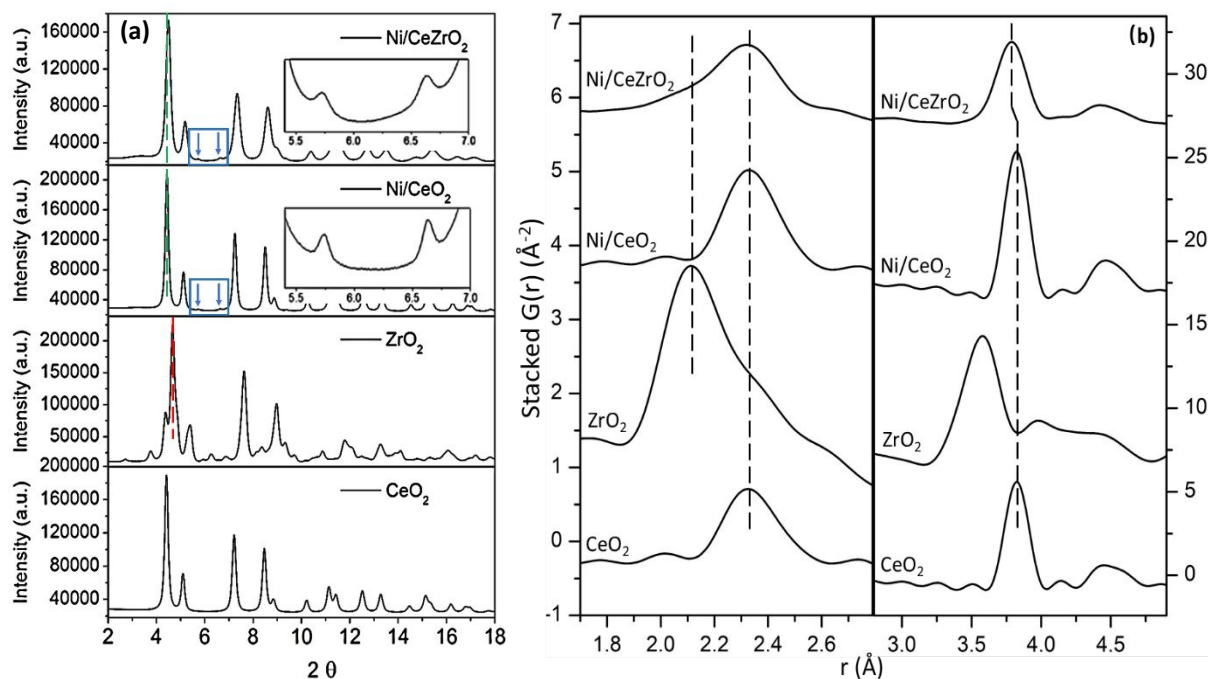


Figure 1. (a) XRD patterns of the synthesized Ni/CeZrO₂ and Ni/CeO₂ samples with ZrO₂ and CeO₂ XRD profiles as references. (b) PDF spectra of Ni/CeZrO₂ and Ni/CeO₂ samples with ZrO₂, CeO₂ PDF profiles as references.

TEM and EDS mapping were conducted for all samples. Figure 2 shows the corresponding images for the post-reaction Ni/CeZrO₂ (Figure 2a) and Ni/CeO₂ (Figure 2b) catalysts in order to investigate the morphology and distributions of Ni/Zr and the influence of the DRM reaction (under stream for 1h at 700 °C). From Figure 2, it is obvious that both Ni and CeO₂ particles in the Ni/CeO₂ sample are larger than those in Ni/CeZrO₂. The particle size for Ni is around 10 and 4 nm in Ni/CeO₂ and Ni/CeZrO₂, respectively, while ceria is around 60 and 30 nm in Ni/CeO₂ and Ni/CeZrO₂, respectively. Meanwhile, Zr preserves its homogeneous distribution, indicating CeZrO₂ mixed oxide maintains its stable structure under the DRM reaction even at 700 °C. Carbon deposition was observed in post reaction Ni/CeO₂ samples (Figure S2) in the form of filamentous fibers and larger carbon composites. Relatively, the Ni/CeZrO₂ sample showed less evidence of total carbon presence.

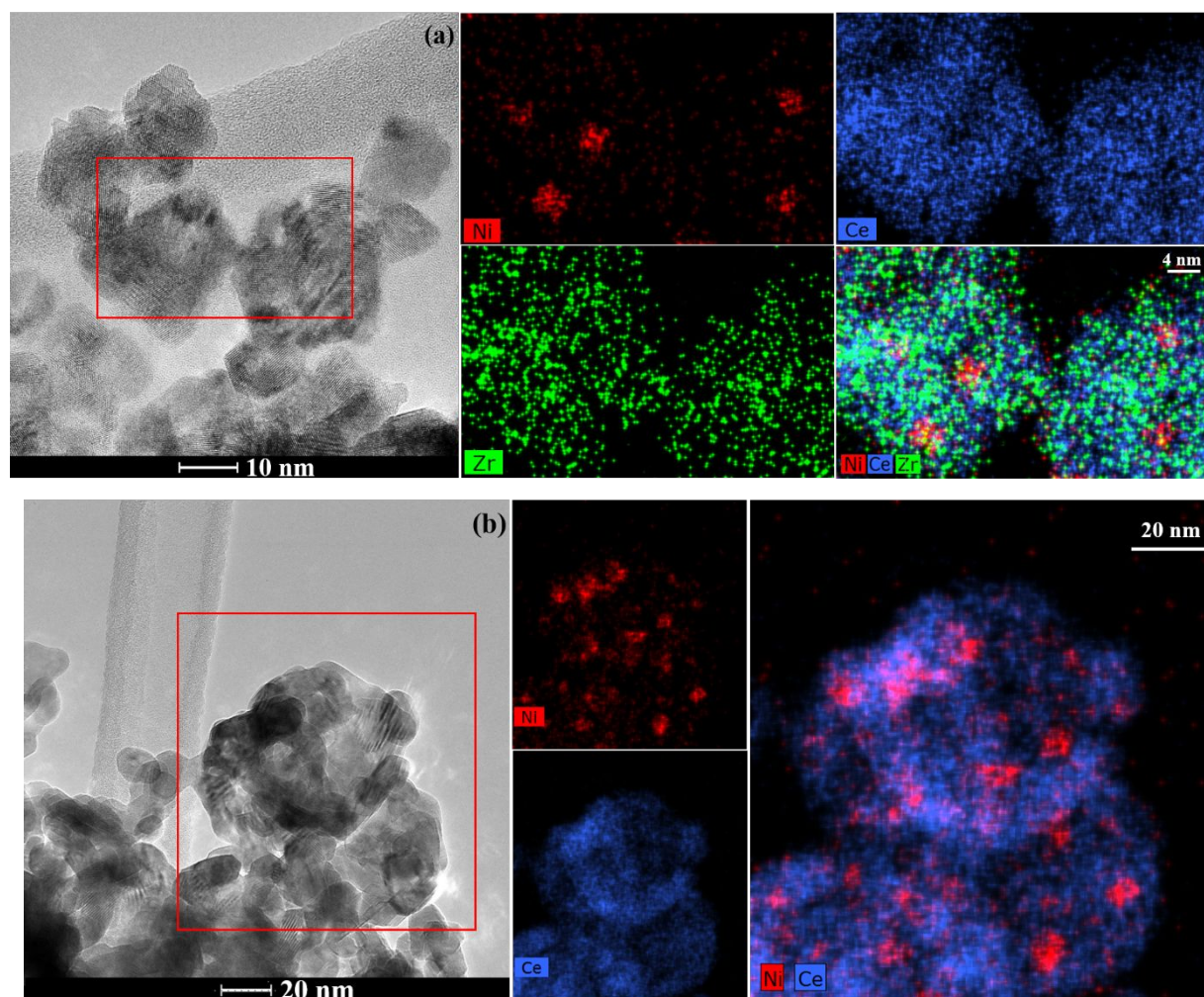


Figure 2. TEM and EDS mapping of Ni/CeZrO₂ catalyst (a) and Ni/CeO₂ catalyst (b) after the DRM reaction at 700 °C.

3.2. Catalytic performance of Ni/CeZrO₂ and Ni/CeO₂ for the DRM reaction . The catalytic performance of both samples was compared through conversion, reaction rate and H₂ selectivity, and the results are presented in Figure 3. Higher DRM reaction activity was observed with Ni/CeZrO₂ than with Ni/CeO₂ through all temperature ranges. At 500 °C, the conversion of CH₄ and CO₂ on Ni/CeZrO₂ was 8% and 15%, respectively, which is close to the thermodynamic equilibrium.³² When the temperature reaches 700 °C, the conversion of CH₄ increased to around 51% and the conversion of CO₂ was 66%; this is ~1.5 times the conversion than that was observed on the Ni/CeO₂ catalyst. Only H₂O, H₂, and CO were detected via GC and RGA (RGA spectra are provided in Figure S3) as the products, and the reaction rate of H₂O, H₂ and CO were 67, 710 and 960 μmol/g_{cat}/s, respectively. The reverse water gas shift reaction (RWGS: H₂ + CO₂ ↔ H₂O

+ CO) is one of the undesirable side reactions accompanying DRM, which consumes a product (H_2) and transforms it to H_2O , thus reducing H_2 selectivity and the H_2/CO stoichiometric ratio.³³⁻³⁴ From Figure 3c, we can see that H_2 selectivity rises with increasing temperature, and, at different temperatures, it remains higher on Ni/CeZrO_2 than on Ni/CeO_2 . This suggests a suppression of the RWGS reaction at higher temperatures with the assistance of Zr in the support.³⁵⁻³⁷ Overall, Ni/CeZrO_2 exhibits better catalytic performance than Ni/CeO_2 , with a higher CH_4 and CO_2 conversion, higher reaction rate, and a higher selectivity for H_2 .

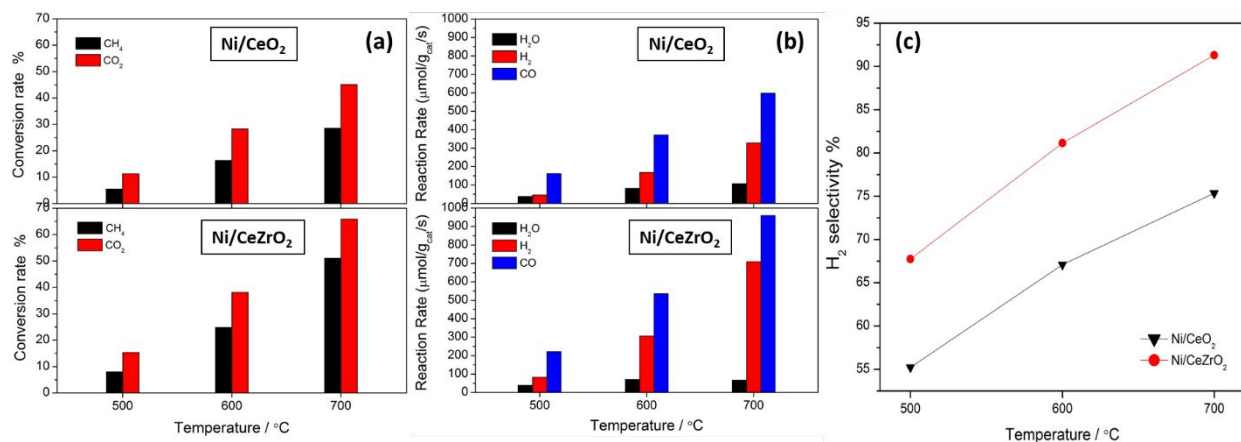


Figure 3. Comparison of the conversion (a), Reaction rate (b), and H_2 selectivity (c) for the DRM reaction over Ni/CeO_2 and Ni/CeZrO_2 samples. Reaction conditions: 10 cc/min CO_2 + 10 cc/min CH_4 + 30 cc/min N_2 with 10 mg of the catalyst; weight hourly space velocity (WHSV): 300,000 $\text{ml}/(\text{g}_{\text{cat}} \cdot \text{h})$.

3.3. Methane activation of the Ni/CeZrO_2 and Ni/CeO_2 catalysts. Figure 4 shows the sequential XRD profiles of the Ni/CeZrO_2 and Ni/CeO_2 samples under a reductive CH_4 atmosphere with a ramping temperature from 25 to 700 °C. The identified NiO (peaks at 5.7° and 6.6°) in the as-prepared samples was reduced at around 400 °C in both Ni/CeZrO_2 and Ni/CeO_2 . As for the CeO_2 support, a significant increase in the intensity of the ceria diffraction peaks for the Ni/CeO_2 sample was observed at high temperatures, while peaks for the Ni/CeZrO_2 sample remained relatively stable. This indicates more pronounced CeO_2 particle sintering in Ni/CeO_2 than in Ni/CeZrO_2 . The evolution of the ceria lattice parameter was obtained from Rietveld refinement (Figure 5). The smaller oxide lattice parameter in Ni/CeZrO_2 sample at room temperature (5.35 vs 5.42 Å for pure ceria) comes from a lattice contraction induced by replacing

Ce⁴⁺ with smaller Zr⁴⁺ in the ceria lattice²⁷⁻²⁹. However, as the temperature increased towards 400 °C, a more substantial ceria lattice expansion was observed in Ni/CeZrO₂ than in Ni/CeO₂. In addition to the linear lattice expansion caused by thermal effects, the abrupt increase of the oxide lattice parameter indicates the reduction of Ce⁴⁺ (1.28 Å ionic radius) to Ce³⁺ (1.48 Å ionic radius) and the repulsion between the oxygen vacancies and their surrounding cations.³⁸⁻⁴⁰ Even though the thermal expansion coefficient (TEC) of zirconia doped ceria was reported to be slightly larger than pure ceria,⁴¹ the conspicuously sharper increase of the ceria lattice in Ni/CeZrO₂ sample around 400 °C suggests a greater reducibility of the ceria support by methane due to the presence of Zr dopants.

Indeed, temperature programmed reduction of Ni/CeO₂ and Ni/CeZrO₂ with H₂ showed that 35% more H₂ was consumed during the reduction of the Ni/CeZrO₂ sample between room temperature and 423 °C (Figure S4), confirming the higher reducibility of CeZrO₂ solid solution support. Notably, an apparent increase of the ceria lattice parameter in the Ni/CeO₂ sample was also detected between 600 and 700 °C under CH₄ atmosphere, and this resulted in a ~ 0.14 Å total expansion (from room temperature to 700 °C) of ceria in Ni/CeO₂, which is comparable to the total lattice expansion of ceria in the CeZrO₂ solid solution (~0.15 Å). This distinct expansion of ceria could be attributed to the bulk reduction of Ce⁴⁺ to Ce³⁺ in Ni/CeO₂ only when the temperature reaches above 600 °C.⁴²⁻⁴³

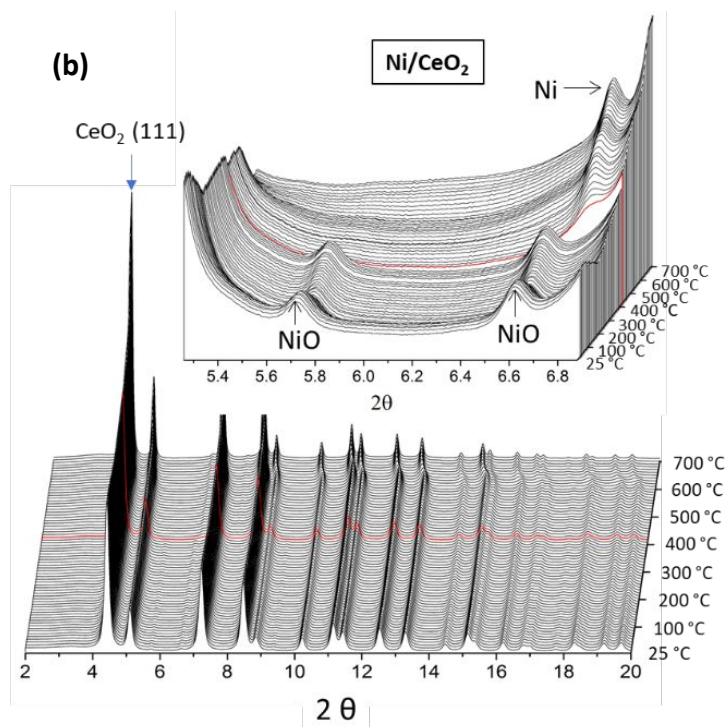
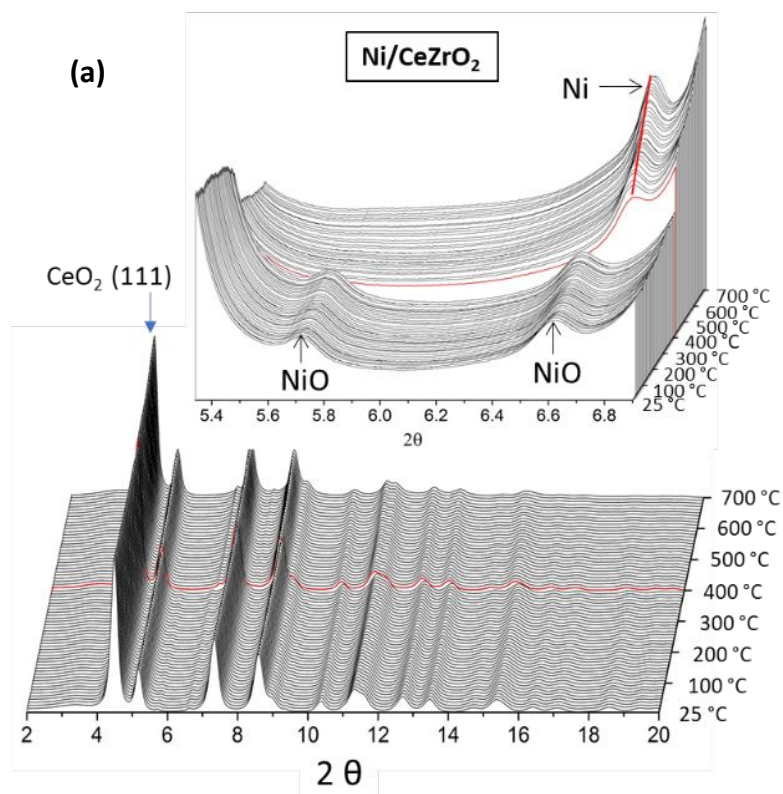


Figure 4. *In-situ* XRD profiles of Ni/CeZrO₂ (a) and Ni/CeO₂ (b) samples in a CH₄ atmosphere. Reaction conditions: 5 cc/min CH₄ + 5 cc/min He, ramping to 700 °C with a 5 °C ramping rate.

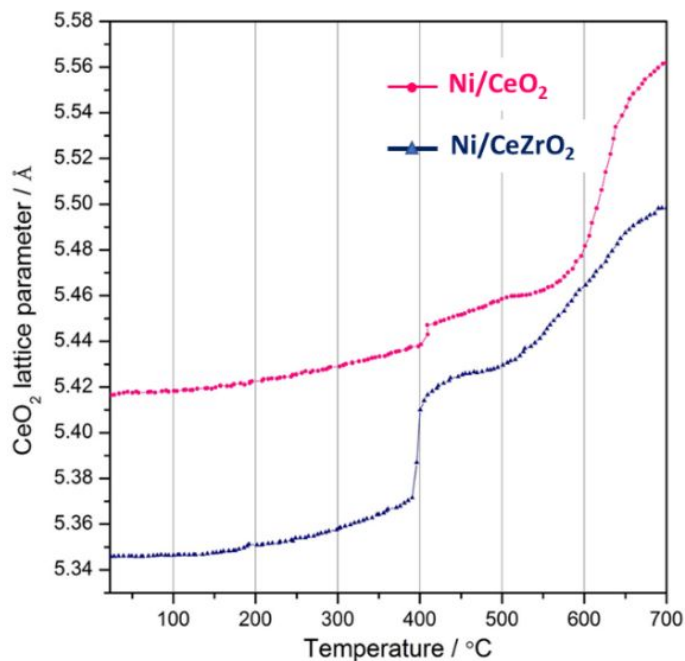


Figure 5. Ceria lattice parameter evolution as a function of temperature during the methane activation process. The results were generated from Rietveld refinement of *in-situ* XRD data using the GSAS-II software.

AP-XPS was conducted to follow the chemical state of the catalysts under methane activation conditions. Ce 3d and Ni 2p AP-XPS spectra for methane activation on Ni/CeZrO₂ and Ni/CeO₂ samples are presented in Figure 6. It is possible to observe a more intense Ce³⁺ peak in Ni/CeZrO₂ than in Ni/CeO₂ at 400 and 500 °C, which validates the *in-situ* XRD results (Figure 5) that ceria is reduced to a larger extent in the Zr-doped support. The reduction of Ni²⁺ to metallic Ni occurs at 400 °C, evident from the AP-XPS spectra for both Ni/CeZrO₂ and Ni/CeO₂ samples, which is also supported by the *in-situ* XRD results (Figure 4). The Ni 2p spectra were also fitted for both samples and the results are provided in Figure S5 and Table S1. The Ni 2p peaks of Ni/CeZrO₂ are noticeably larger and narrower than those of Ni/CeO₂. With the same loading of Ni in both samples, the larger and narrower Ni 2p peak in Ni/CeZrO₂ suggests that more Ni⁰ sites with smaller Ni⁰ particles were exposed on this sample's surface when compared to the Ni/CeO₂. In the Ni/CeZrO₂, a higher dispersion of smaller Ni particles is due to a more defect rich and reactive

oxide support. The Zr 3d spectra were also collected and presented in Figure S6a, showing a stable Zr^{4+} chemical state throughout the entire reaction with methane.

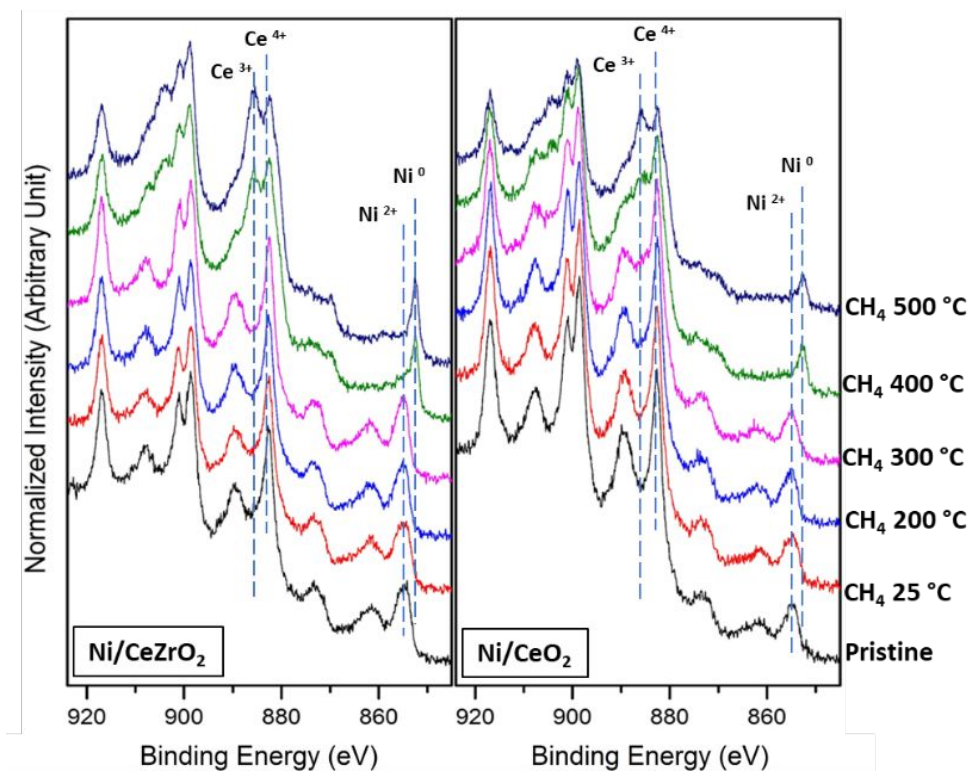


Figure 6. Ce 3d and Ni 2p AP-XPS spectra of Ni/CeZrO₂ and Ni/CeO₂ samples in a CH₄ atmosphere at elevated temperatures. Reaction conditions: 30 mTorr of CH₄ at temperatures of 25, 200, 300, 400, and 500 °C.

3.4. Dry Reforming of Methane on the Ni/CeZrO₂ and Ni/CeO₂ catalysts. We employed *in-situ* XANES and XRD measurements to elucidate the chemical and structural changes that occurred during the DRM reaction on the Ni/CeZrO₂ and Ni/CeO₂ catalysts. These results are shown in Figures 7a and 8, respectively. NiO was identified in the as-prepared Ni/CeZrO₂ and Ni/CeO₂ samples with both techniques, and it was reduced to metallic Ni during the H₂ pretreatment process (Figure 7a and Figure 8). The reduction temperatures of NiO during H₂ pretreatment were close for both samples (Figure 8), with Ni/CeZrO₂ (~280 °C) slightly higher than Ni/CeO₂ (~260 °C). The reduced Ni⁰ maintains its metallic nature under the DRM reaction (CO₂ + CH₄ + He) from 500 to 700 °C, according to both XANES and XRD profiles in Figure 7a and 8, respectively.

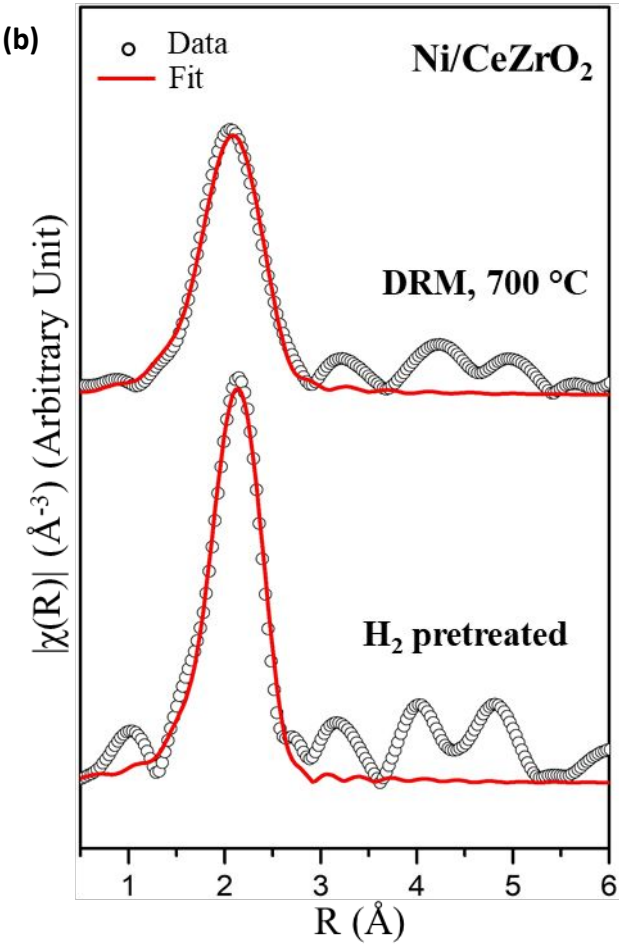
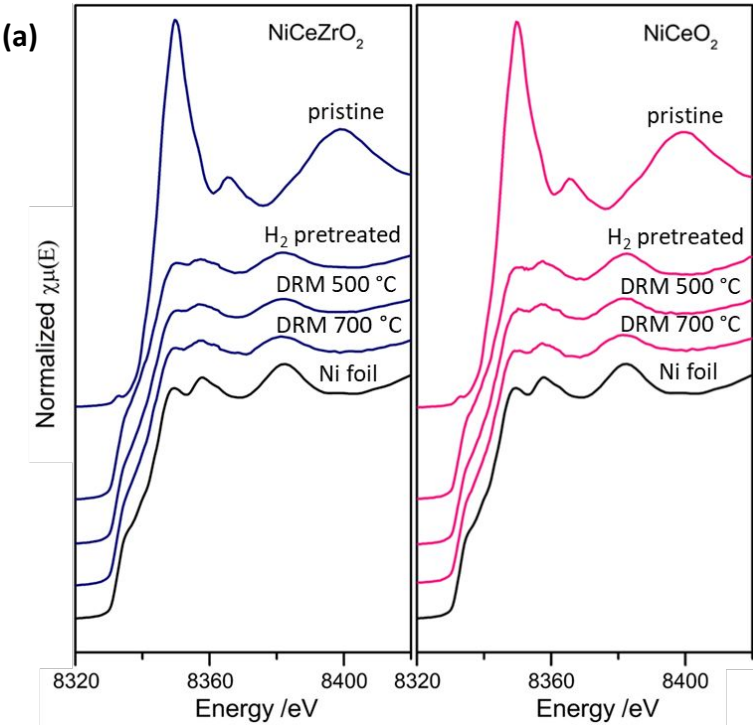
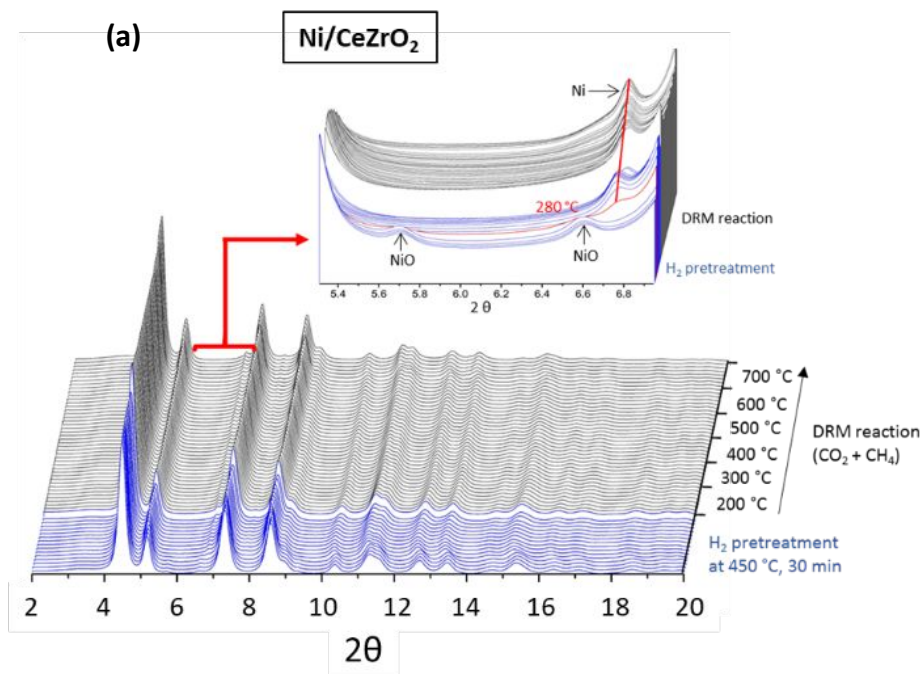


Figure 7. (a) *In-situ* Ni K-edge XANES spectra of Ni/CeO₂ and Ni/CeZrO₂ samples with Ni foil spectra provided as the reference. (b) The Fourier-transformed R-space EXAFS spectra of Ni/CeZrO₂ sample after H₂ pretreatment and during the DRM reaction at 700 °C. (The catalyst (~ 2 mg) was pretreated in H₂ at 450 °C for 30 min before switching the gas to a mixture of 2 cc/min CO₂ + 2 cc/min CH₄ + 6 cc/min He at room temperature. The sample was then heated under DRM reaction atmosphere from 25 to 700 °C with a 10 °C/min ramping rate. XAFS spectra were collected before and after H₂ pretreatment at 25 °C, and under the DRM reaction condition at 25, 500 and 700 °C.



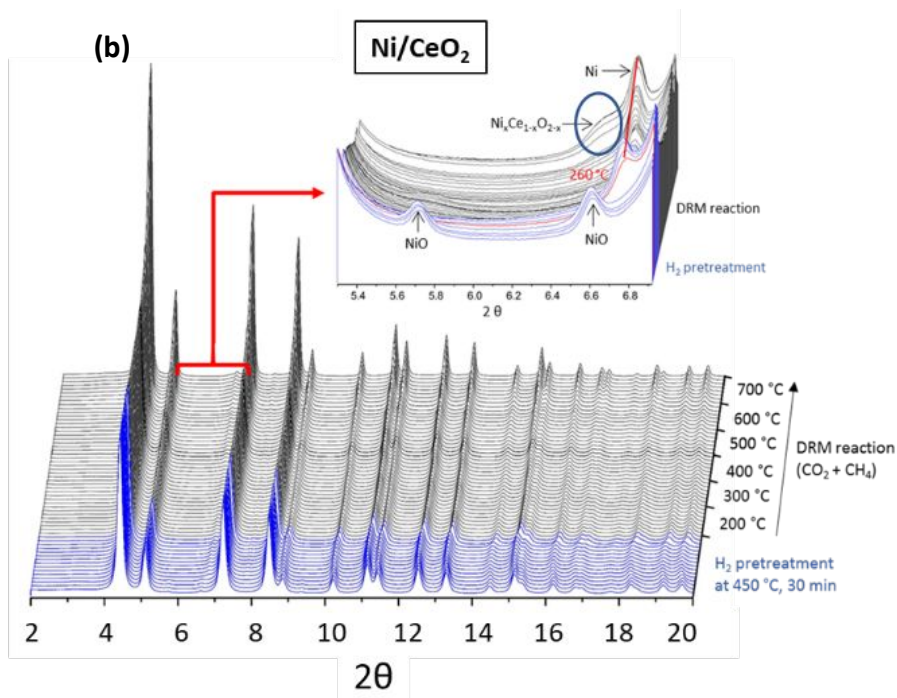


Figure 8. *In-situ* XRD profiles of Ni/CeZrO₂ (a) and Ni/CeO₂ (b) samples under DRM reaction conditions. The catalyst was pretreated in H₂ at 450 °C for 30 min before switching the gas to a mixture of 2 cc/min CO₂ + 2 cc/min CH₄ + 6 cc/min He at room temperature. The sample was then heated under DRM reaction atmosphere from 25 to 700 °C with a 10 °C/min ramping rate and 30 min soak time at each temperature stage of 200, 300, 400, 500, 600, and 700 °C).

The CeO₂ particle sintering was also observed for the Ni/CeO₂ sample during the methane dry reforming reaction (Figure 8b and 9a) as seen in pure methane (Figure 4b). The Rietveld refinement results in Figure 9a illustrate that the crystallite size of ceria in the Ni/CeO₂ sample increased from 16 to 60 nm at 700 °C while the corresponding increase of the ceria crystallite size in Ni/CeZrO₂ was only ~ 14 nm (increasing from 19 to 33 nm). The crystallite sizes of ceria support calculated by the Rietveld refinement are also consistent with the EDS mapping results shown in Figure 2, indicating that the ceria particles in both samples are all crystalline. Figure 9b demonstrates that the lattice parameter of ceria in Ni/CeZrO₂ is always smaller than that in the Ni/CeO₂ sample during the reaction below 700 °C. This can be attributed to the introduction of smaller Zr⁴⁺ ions into ceria support which also creates a contraction strain and decrease of the total ceria lattice parameter.²⁷⁻²⁹ However, when the temperature increased to 700 °C during DRM, the initially smaller ceria lattice in the Ni/CeZrO₂ sample expanded significantly to a value even

larger than the ceria lattice parameter of the Ni/CeO₂. This expansion signifies the severe reduction of the ceria support in the Ni/CeZrO₂ sample when the temperature reached 700 °C under the DRM reaction condition,^{38-39, 42-43} indicating the improved reducibility of the ceria support with Zr dopants.

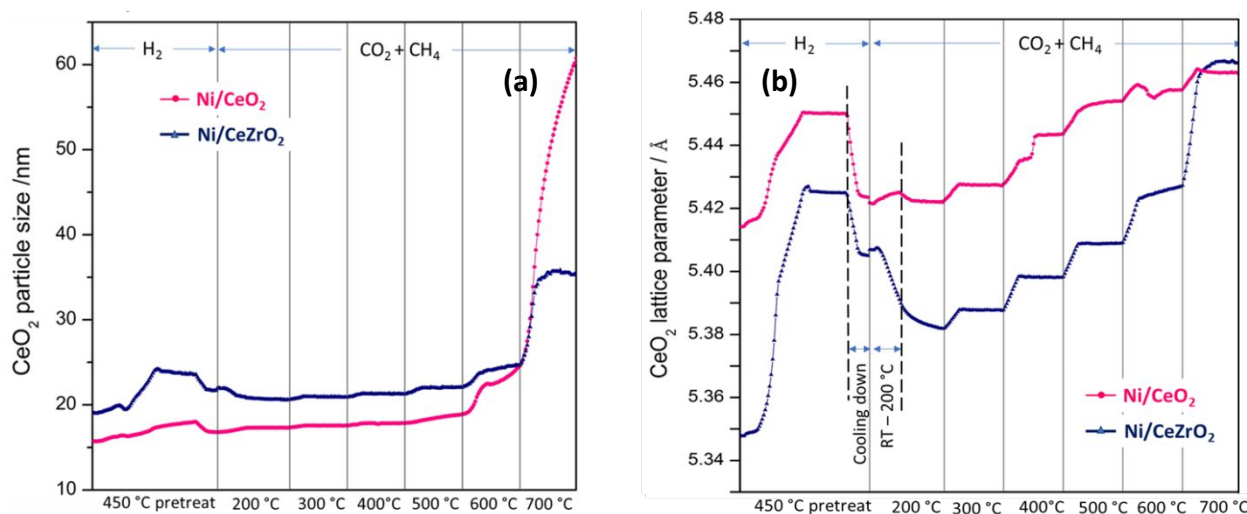


Figure 9. (a) Ceria particle size and (b) Ceria lattice parameter evolution during the methane dry reforming reaction. The results were generated from Rietveld refinement of the *in-situ* XRD data using the GSAS-II software.

The particle size of the active metallic Ni phase during the DRM reaction was also evaluated by Rietveld refinement and EXAFS fitting for Ni⁰ particles in the Ni/CeO₂ and Ni/CeZrO₂ samples. The Fourier-transformed R-space EXAFS spectra of both Ni/CeZrO₂ and Ni/CeO₂, are presented in Figure 7b and Figure S7, respectively and the fitting parameters are displayed in Table S2. The fitted coordination numbers of Ni atoms in the Ni/CeO₂ sample are 10.6 and 11.9 for the H₂ pretreated and under the DRM reaction at 700 °C, respectively, which are above the limit for the accurate estimation of the particle size using the half-sphere fcc packing model⁴⁴. However, for the Ni/CeO₂, the metallic Ni diffraction peaks (Figure 8b) are relatively larger and more intense than those in the Ni/CeZrO₂ (Figure 8a), thus enabling the Rietveld refinement to be performed on the Ni phase in Ni/CeO₂ to get an accurate Ni crystallite size. As for the Ni/CeZrO₂ sample, the smaller and broader diffraction peaks of the Ni phase make it difficult for accurate Rietveld refinement, thus EXAFS fittings were performed to obtain the coordination number of the Ni atoms and the results were further used to estimate the Ni particle size in the

Ni/CeZrO₂ catalyst, using the half-sphere fcc packing model.⁴⁴ Both the less pronounced Ni phase diffraction peaks and the small Ni atom coordination number in Ni/CeZrO₂ indicate smaller Ni particles than those in Ni/CeO₂, which is verified by the summarized EXAFS fitting and Rietveld refinement results in Table 1. The metallic Ni particles in Ni/CeZrO₂ during the DRM reaction were estimated to be around 2.4 nm at room temperature and only increased to 3.5 nm at 700 °C. The Ni⁰ particles in Ni/CeZrO₂ are smaller and exhibit a lower particle sintering extent at 700°C under the DRM reaction, whereas the crystallite size of Ni/CeO₂ (calculated by Rietveld refinement) was 8 nm at room temperature and sintered to 11 nm at 700 °C. It should be pointed out that the estimation of the Ni particle size using the half-sphere fcc packing model⁴⁴ at 700 °C might result in a smaller Ni particle size due to the variation of the Debye–Waller factor at high temperatures than 25 °C. However, the estimated Ni particle size using either Rietveld refinement or the XAFS fitting agrees well with the particle size obtained from the TEM and EDS mapping images shown in Figure 2, suggesting that our methods for calculating the particle size are reliable. These results indicate that the presence of Zr in the ceria support improves the dispersion of Ni particles on the surface as well as diminishes Ni particle sintering at high temperature during the DRM reaction.

Table 1. Metallic Ni particle size in the Ni/CeZrO₂ and Ni/CeO₂ sample during the DRM reaction.

Ni ⁰ particle size (nm)	DRM at 25 °C	DRM at 700 °C
Ni/CeZrO ₂	2.4*	3.5*
Ni/CeO ₂	8#	11#

* Calculated by EXAFS fitting; # Calculated by Rietveld refinement

Noticeably, a set of additional diffraction peaks at 4.0 ° and 6.5 ° appeared in the Ni/CeO₂ sample at 600 °C and intensified when the temperature increased to 700 °C (blue circled area in Figure 8b and the selected representative *in-situ* XRD patterns in Figure 10). This set of peaks could be assigned to a new ceria phase with an expanded lattice parameter (5.99 Å compared to 5.46 Å of the main ceria structure). As can be seen in Table 2, the peak at 4.0° with an interplanar spacing of 3.46 Å can be associated with the expanded (111) plane of the main structure ceria in the Ni/CeO₂ sample. The peak at 6.5° (d-spacing 2.12 Å) corresponds to the expanded (220) plane comparing to the main structure ceria peak at 7.2° (d-spacing 1.93 Å). The relationship between

the assigned (111) and (220) planes in the emerged new phase satisfied the structural relationship in the standard ceria face-cubic-centered structure, in which d_{111}/d_{220} equals to $2\sqrt{2}/\sqrt{3}$. This substantiates that our assignment of the emerged additional diffraction peaks to a lattice-expanded ceria phase is reasonable. The expansion of the ceria lattice in this new emerged phase could further be attributed to a migration of the surface Ni atoms into the ceria lattice, which partially replace the cerium sites. When a Ce^{4+} is substituted by a Ni^{2+} , an oxygen vacancy is created simultaneously to sustain the charge neutrality of the sample, and as previously discussed, the repulsion force between the oxygen vacancies and their surrounding cations consequently lead to the ceria lattice expansion.^{39, 45-46} Thus, according to the above discussion, the set of additional diffraction peaks at 4.0° and 6.5° can be attributed to a partially doped nickel-ceria solid solution, $\text{Ce}_{1-x}\text{Ni}_x\text{O}_{2-y}$. This type of mixed-oxide has been seen after heating mechanical mixtures of NiO- CeO_2 .⁴⁷⁻⁴⁹ Diffraction peaks related to a $\text{Ce}_{1-x}\text{Ni}_x\text{O}_{2-y}$ solid solution in Ni/CeZrO₂ (Figure 8a) are not as evident as in the Ni/CeO₂ sample. This implies that the introduction of Zr into the ceria support could inhibit or mitigate the diffusion of Ni into the ceria lattice and maintain the active metallic Ni phase on the surface.

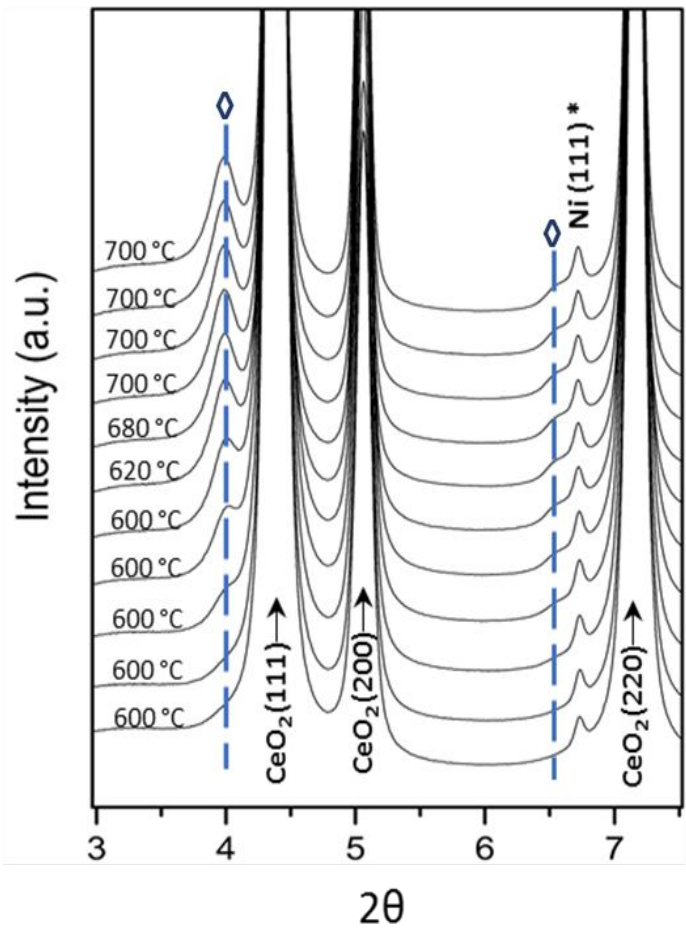


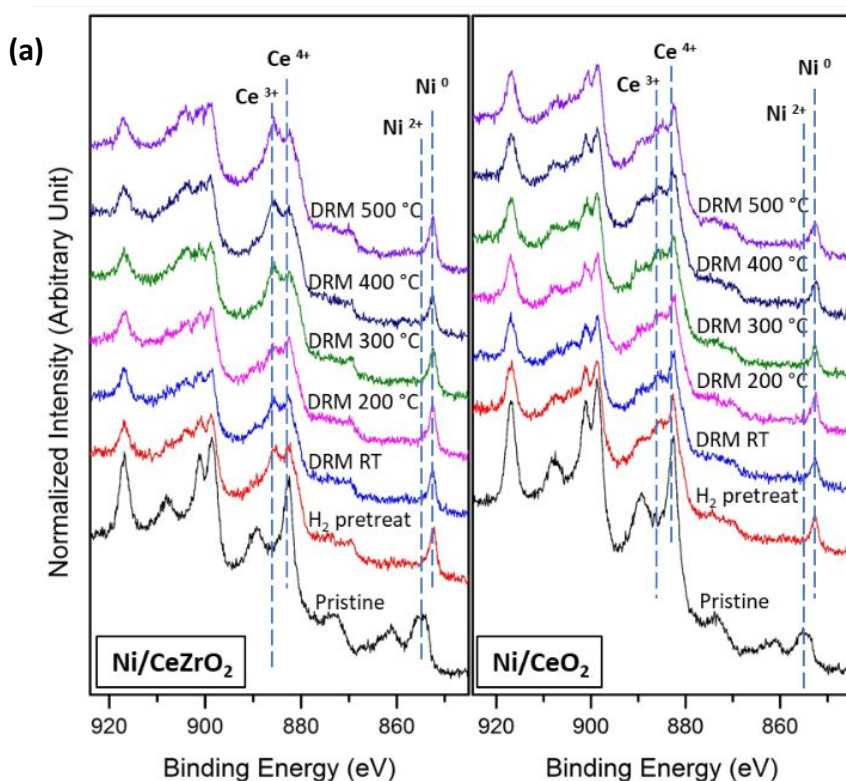
Figure 10. Selected *in-situ* XRD patterns of Ni/CeO₂ sample at and above 600 °C. The blue dashed lines mark out the emergence of a crystalline Ce_{1-x}Ni_xO_{2-y} solid solution phase inside the Ni/CeO₂ sample during the DRM reaction at and above 600 °C.

Table 2. Interplanar spacing of main structure CeO₂ and the emerged new phase.

d-spacing (Å)	(111)	(220)	d ₁₁₁ /d ₂₂₀ (2√2/√3)
main CeO ₂	3.15	1.93	1.63
emerged phase (◊)	3.46	2.12	1.63

AP-XPS measurements were also performed on the Ni/CeZrO₂ and Ni/CeO₂ samples to monitor the dynamic changes of the sample surface under the DRM reaction conditions. The data for the Ce 3d and Ni 2p spectra of both samples are plotted in Figure 11a. As was observed in the *in-situ* XRD experiment, NiO was reduced to Ni⁰ after H₂ reduction and the metallic Ni phase remained reduced during the DRM reaction at elevated temperatures for both Ni/CeO₂ and Ni/CeZrO₂. The

less intense and broader Ni peaks in the Ni/CeO₂ sample suggests that less Ni sites (25% lower Ni peak area in Ni/CeO₂ than in Ni/CeZrO₂) are exposed on the surface which was also observed in the Ni 2p AP-XPS spectra in a CH₄ atmosphere (Figure 6). Ce 3d spectra were fitted with Ce⁴⁺ and Ce³⁺ components (see Figure S8 and Table S3), and the concentration of Ce³⁺ in both samples is plotted in Figure 11b. As can be seen from the plot, the ceria support was reduced after H₂ pretreatment for both samples, with a stronger Ce³⁺ feature present in Ni/CeZrO₂ than in Ni/CeO₂. The amount of Ce³⁺ in Ni/CeO₂ near the sample surface remains at ~30%, which indicates that a dynamic equilibrium exists between the reduction and oxidation process exerted by CH₄ and CO₂ on the ceria surface, respectively. However, the surface Ce³⁺ in Ni/CeZrO₂ sample was around 35% after H₂ reduction, and increased to ~43% when the temperature reached 300 °C, followed by a further slight increase to 45% at 500 °C. The higher fraction of Ce³⁺ in Ni/CeZrO₂ sample during the DRM reaction reinforced the previous explanation that the introduction of Zr into the ceria support increases the reducibility of the support. Zr 3d spectra are also provided in Figure S7b, showing that Zr maintains a 4+ oxidation state throughout the whole DRM reaction and does not appear to be involved in the reaction through changes of its own oxidation state.



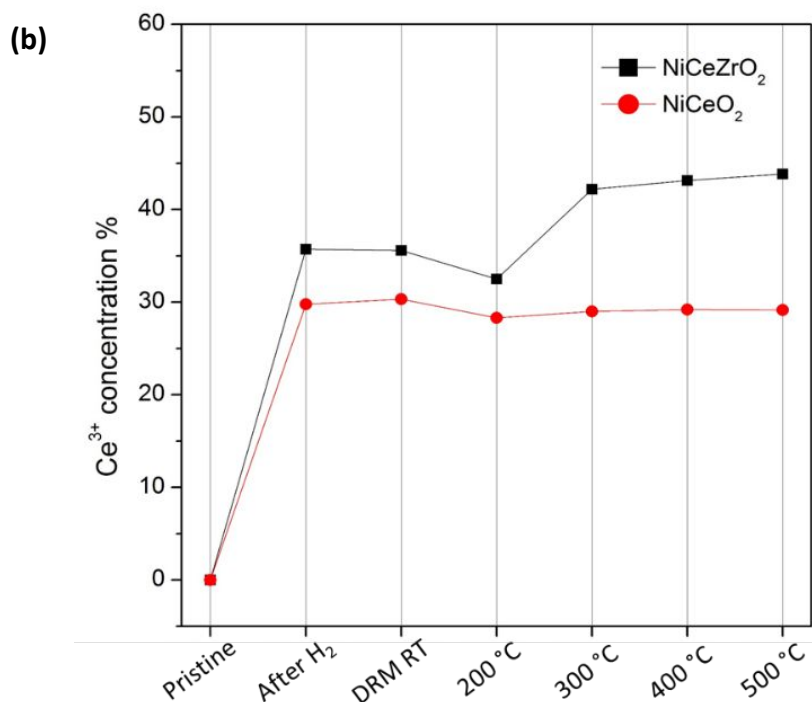


Figure 11. (a) Ce 3d and Ni 2p AP-XPS spectra of Ni/CeZrO₂ and Ni/CeO₂ samples under DRM reaction atmosphere at elevated temperatures. (b) Fraction of Ce³⁺ in the catalysts at different temperatures under DRM conditions. Reaction conditions: 20 mTorr of H₂ were used to pretreat the samples at 450 °C for 30 min in the analysis chamber. After pumping down the H₂, a 60 mTorr CH₄ + CO₂ 1:1 gas mixture was introduced into analysis chamber, and the spectra were collected at 25, 200, 300, 400 and 500 °C under this gas mixture. The Ce³⁺ concentration was obtained through the AP-XPS spectra fitting and the error (% StDev) is below 5%, please refer to the supporting information for additional information.

The results presented above demonstrate that upon incorporation of Zr into the ceria support, the reducibility of this oxide was enhanced, which agrees with previously reported results.^{29, 50-51} Furthermore, the improved reducibility facilitates CH₄ activation on the ceria surface as confirmed by the ceria lattice parameter changes during the *in-situ* XRD CH₄ activation measurement (Figure 5) and the AP-XPS results (Figure 6); It also results in a higher Ce³⁺ content after H₂ pretreatment and under the DRM reaction conditions (Figure 11). In previous studies, the Ce³⁺ was found to be the active site for CO₂ activation and oxidation of carbon species covering the surface of the catalyst during the DRM reaction.^{9-10, 52} Thus, with more Ce³⁺ present in ceria-

zirconia support, the CO₂ activation process was enabled, resulting in an elevated CO₂ conversion rate, and the carbon species on the Ni/CeZrO₂ sample surface was also decreased. The existence of Zr in the ceria support also helps to disperse metallic Ni particles (Figure 2 and Table 1) and maintains the structure of the ceria support. The latter is apparent by the relatively stable ceria particle size during the DRM reaction (Figure 9a) and the absence of Ni incorporation into the ceria support in the Ni/CeZrO₂ catalyst (Figure 8). The structurally stable ceria-zirconia support further helps to maintain a larger Ce³⁺ content with more oxygen vacancies. Additionally it stabilizes the smaller metallic Ni particles, preserving their higher dispersion and adequate metallic nature on the sample surface.⁵³⁻⁵⁴ Furthermore, throughout the DRM reaction, the small and stable Ni particles indicate a stronger metal-support interaction between Ni and the Zr doped ceria support. With the help of this strong interaction, metallic Ni particles appear rigidly anchored on the CeZrO₂ support, which inhibits particle sintering even at higher temperatures (up to 700 °C). Metallic Ni plays an pivotal role in the direct dissociation of CH₄, and metal/support interfacial sites are claimed to be the active sites in CH₄ and CO₂ activation through redox reactions.^{21, 55} Higher dispersion of metallic Ni particles on the sample surface provides more metallic Ni sites and metal/support interfacial sites available for interaction with CH₄ and CO₂ reactant gases. These sites, combined with the metal-support interaction, which promotes the electron and oxygen mobility in the catalyst, lead to an improved turnover of CH₄ and CO₂ and higher production rate of CO + H₂.^{10, 52, 56-57}

CONCLUSION

In this work the effects of Zr-doping of the ceria support for the methane dry reforming reaction was comprehensively investigated on Ni/CeO₂ and Ni/CeZrO₂ catalysts. By introducing Zr as the dopant, the catalytic performance including conversion, reaction rate, and H₂ selectivity were significantly enhanced. The *in-situ* characterizations of the catalysts during difficult DRM reaction conditions depict the dynamic chemical and structural changes Ni and Ce go through, with and without the Zr dopant. The results reveal details about the mechanism for the enhanced DRM catalytic performance achieved with Zr doping. By doping Zr into the ceria support, a larger Ce³⁺ content was observed in the mixed-oxide support upon reaction with pure CH₄ or during DRM, indicating a higher reducibility of the mixed-oxide support. The particle sintering process of both Ni and ceria was effectively hindered. A stable ceria structure with the Zr dopant was

preserved without any active metallic Ni incorporation into the support. The smaller nickel particles expose a larger amount of active metallic Ni surface and Ni-CeO₂ interfacial sites for CH₄ and CO₂ activation. The small and well-dispersed metallic Ni particles interact strongly with the highly reduced, yet structurally stable, ceria-zirconia support in the Ni/CeZrO₂ catalysts. All of this coalesces to result in an enhanced reaction activity and H₂ selectivity for the dry reforming of methane reaction.

ASSOCIATED CONTENT

Calculations of the conversions, reaction rates and selectivity; PDF spectra of Ni/CeZrO₂ and Ni/CeO₂ samples with ZrO₂, CeO₂ PDF profiles as references; TEM images of the Ni/CeO₂ sample after the DRM reaction at 700 °C for 1h; Residual gas analyzer spectra of the Ni/CeZrO₂ and Ni/CeO₂ under the DRM reaction; Temperature programmed reduction (H₂-TPR) of Ni/CeO₂ and 4 Ni/CeZrO₂ catalysts; Fitted Ni 2p AP-XPS spectra of Ni/CeZrO₂ and Ni/CeO₂ samples under CH₄ atmosphere with elevated temperatures and the fitting results; AP-XPS results of Zr 3d spectra during CH₄-temperature programmed reduction and DRM reaction process; The Fourier-transformed R-space EXAFS spectra and Ni K-edge EXAFS fitting results of Ni/CeO₂ and Ni/CeZrO₂ samples after H₂ pretreatment and under DRM reaction at 700 °C; Fitted Ce 3d AP-XPS spectra of Ni/CeZrO₂ and Ni/CeO₂ samples under DRM reaction condition and the fitting results and details.

ACKNOWLEDGEMENTS

The work carried out at Brookhaven National Laboratory was supported by the US Department of Energy under contract no. DE-SC0012704. S.D.S. is supported by a US Department of Energy Early Career Award. The PDF measurement used resources 28ID-1 of the National Synchrotron Light Source II, a U.S. Department of Energy (DOE) Office of Science User Facility operated for the DOE Office of Science by Brookhaven National Laboratory under Contract No. DE-SC0012704. This research also used resources of the Center for Functional Nanomaterials, specifically the electron microscopy facilities which is a U.S. DOE Office of Science Facility, at Brookhaven National Laboratory under Contract No. DE-SC0012704. The XRD and XAFS experiments used resources of the Advanced Photon Source Beamline 17BM (XRD) and 20ID (XAFS) at Argonne National Laboratory, which is an Office of Science User Facility operated

for the U.S. Department of Energy (DOE) Office of Science and was supported by the U.S. DOE under Contract No. DE-AC02-06CH11357, and the Canadian Light Source and its funding partners. Janvit Teržan, Kristijan Lorber, and Petar Djinić are funded by Slovenian national research agency (ARRS) through research program P2-150 and projects J2-1726 and BI-US/18-20-004.

REFERENCES

1. Aramouni, N. A. K.; Touma, J. G.; Tarboush, B. A.; Zeaiter, J.; Ahmad, M. N. *Catalyst design for dry reforming of methane: Analysis review. Renew. Sust. Energ. Rev.* **2018**, *82*, 2570-2585.
2. Jang, W.-J.; Shim, J.-O.; Kim, H.-M.; Yoo, S.-Y.; Roh, H.-S. *A review on dry reforming of methane in aspect of catalytic properties. Catal. Today* **2019**, *324*, 15-26.
3. Ross, J. R. H. *Contemporary Catalysis*, Ross, J. R. H., Ed. Elsevier: Amsterdam, 2019, 251-272.
4. Pachauri, R. K.; Allen, M. R.; Barros, V. R.; Broome, J.; Cramer, W.; Christ, R.; Church, J. A.; Clarke, L.; Dahe, Q.; Dasgupta, P. *Climate change 2014: synthesis report. Contribution of Working Groups I, II and III to the fifth assessment report of the Intergovernmental Panel on Climate Change*. Ipcc: 2014.
5. Fan, M. S.; Abdullah, A. Z.; Bhatia, S. *Catalytic technology for carbon dioxide reforming of methane to synthesis gas. ChemCatChem* **2009**, *1*, 192-208.
6. Cavenati, S.; Grande, C. A.; Rodrigues, A. E. *Separation of CH₄/CO₂/N₂ mixtures by layered pressure swing adsorption for upgrade of natural gas. Chem. Eng. Sci.* **2006**, *61*, 3893-3906.
7. Zhang, F.; Liu, Z.; Zhang, S.; Akter, N.; Palomino, R. M.; Vovchok, D.; Orozco, I.; Salazar, D.; Rodriguez, J. A.; Llorca, J. *In Situ Elucidation of the Active State of Co–CeO_x Catalysts in the Dry Reforming of Methane: The Important Role of the Reducible Oxide Support and Interactions with Cobalt. ACS.Catal.* **2018**, *8*, 3550-3560.
8. Zhang, F.; Yao, S.; Liu, Z.; Gutiérrez, R. A.; Vovchok, D.; Cen, J.; Xu, W.; Ramírez, P. J.; Kim, T.; Senanayake, S. D.; Rodriguez, J. A. *Reaction of Methane with MO_x/CeO₂ (M = Fe, Ni, and Cu) Catalysts: In Situ Studies with Time-Resolved X-ray Diffraction. J. Phys. Chem. C* **2018**, *122*, 28739-28747.
9. Liu, Z.; Grinter, D. C.; Lustemberg, P. G.; Nguyen-Phan, T.-D.; Zhou, Y.; Luo, S.; Waluyo, I.; Crumlin, E. J.; Stacchiola, D. J.; Zhou, J.; Carrasco, J.; Busnengo, H. F.; Ganduglia-Pirovano, M. V.; Senanayake, S. D.; Rodriguez, J. A. *Dry Reforming of Methane on a Highly-Active Ni-CeO₂ Catalyst: Effects of Metal-Support Interactions on C–H Bond Breaking. Angew. Chem. Int. Ed.* **2016**, *128*, 7581-7585.
10. Liu, Z.; Zhang, F.; Rui, N.; Li, X.; Lin, L.; Betancourt, L. E.; Su, D.; Xu, W.; Cen, J.; Attenkofer, K.; Idriss, H.; Rodriguez, J. A.; Senanayake, S. D. *Highly Active Ceria-Supported Ru Catalyst for the Dry Reforming of Methane: In Situ Identification of Ru^{δ+}–Ce³⁺ Interactions for Enhanced Conversion. ACS.Catal.* **2019**, *9*, 3349-3359.
11. Farmer, J. A.; Campbell, C. T. *Ceria Maintains Smaller Metal Catalyst Particles by Strong Metal-Support Bonding. Science* **2010**, *329*, 933-936.
12. Basile, F.; Mafessanti, R.; Fasolini, A.; Fornasari, G.; Lombardi, E.; Vaccari, A. *Effect of synthetic method on CeZr support and catalytic activity of related Rh catalyst in the oxidative reforming reaction. J. Eur. Ceram. Soc.* **2019**, *39*, 41-52.
13. Djinić, P.; Črnivec, I. G. O.; Pintar, A. *Biogas to syngas conversion without carbonaceous deposits via the dry reforming reaction using transition metal catalysts. Catal. Today* **2015**, *253*, 155-162.
14. Wang, Y.; Liang, S.; Cao, A.; Thompson, R. L.; Veser, G. *Au-mixed lanthanum/cerium oxide catalysts for water gas shift. Appl. Catal., B* **2010**, *99*, 89-95.

15. Liu, Z.; Xu, W.; Yao, S.; C. Johnson-Peck, A.; Zhao, F.; Michorczyk, P.; Kubacka, A.; Stach, E.; Fernández-García, M.; Senanayake, S.; A. Rodriguez, J. *Superior performance of Ni–W–Ce mixed-metal oxide catalysts for ethanol steam reforming: Synergistic effects of W- and Ni-dopants*. *J. Catal.* **2015**, 321, 90-99.
16. Razzaq, R.; Zhu, H.; Jiang, L.; Muhammad, U.; Li, C.; Zhang, S. *Catalytic methanation of CO and CO₂ in coke oven gas over Ni–Co/ZrO₂–CeO₂*. *Ind. Eng. Chem. Res.* **2013**, 52, 2247-2256.
17. Le, M. C.; Van, K. L.; Nguyen, T. H. T.; Nguyen, N. H. *The Impact of Ce-Zr Addition on Nickel Dispersion and Catalytic Behavior for CO₂ Methanation of Ni/AC Catalyst at Low Temperature*. *J. Chem.* **2017**, 2017, 11.
18. Kambolis, A.; Matralis, H.; Trovarelli, A.; Papadopoulou, C. *Ni/CeO₂-ZrO₂ catalysts for the dry reforming of methane*. *Appl. Catal., A* **2010**, 377, 16-26.
19. Wang, F.; Xu, L.; Yang, J.; Zhang, J.; Zhang, L.; Li, H.; Zhao, Y.; Li, H. X.; Wu, K.; Xu, G. Q.; Chen, W. *Enhanced catalytic performance of Ir catalysts supported on ceria-based solid solutions for methane dry reforming reaction*. *Catal. Today* **2017**, 281, 295-303.
20. Mullen, G. M.; Evans, E. J.; Siegert, B. C.; Miller, N. R.; Rosselet, B. K.; Sabzevari, I.; Brush, A.; Duan, Z.; Buddie Mullins, C. *The interplay between ceria particle size, reducibility, and ethanol oxidation activity of ceria-supported gold catalysts*. *React. Chem. Eng.* **2018**, 3, 75-85.
21. Boaro, M.; Colussi, S.; Trovarelli, A. *Ceria-Based Materials in Hydrogenation and Reforming Reactions for CO(2) Valorization*. *Front. Chem.* **2019**, 7, 28-28.
22. Farrow, C.; Juhas, P.; Liu, J.; Bryndin, D.; Božin, E.; Bloch, J.; Proffen, T.; Billinge, S. *PDFfit2 and PDFgui: computer programs for studying nanostructure in crystals*. *J. Phys.: Condens. Matter* **2007**, 19, 335219.
23. Chupas, P. J.; Chapman, K. W.; Kurtz, C.; Hanson, J. C.; Lee, P. L.; Grey, C. P. *A versatile sample-environment cell for non-ambient X-ray scattering experiments*. *J. Appl. Crystallogr.* **2008**, 41, 822-824.
24. Toby, B. H.; Von Dreele, R. B. *GSAS-II: the genesis of a modern open-source all purpose crystallography software package*. *J. Appl. Crystallogr.* **2013**, 46, 544-549.
25. Ravel, B.; Newville, M. *ATHENA, ARTEMIS, HEPHAESTUS: data analysis for X-ray absorption spectroscopy using IFEFFIT*. *J. Synchrotron Radiat.* **2005**, 12, 537-541.
26. Palomino, R. M.; Hamlyn, R.; Liu, Z.; Grinter, D. C.; Waluyo, I.; Rodriguez, J. A.; Senanayake, S. D. *Interfaces in heterogeneous catalytic reactions: Ambient pressure XPS as a tool to unravel surface chemistry*. *J. Electron Spectrosc. Relat. Phenom.* **2017**, 221, 28-43.
27. Sadykov, V. A.; Simonov, M. N.; Mezentseva, N. V.; Pavlova, S. N.; Fedorova, Y. E.; Bobin, A. S.; Bepalko, Y. N.; Ishchenko, A. V.; Krieger, T. A.; Glazneva, T. S.; V., L. T.; Cherepanova, S. V.; Kaichev, V. V.; Saraev, A. A.; Chesalov, Y. A.; Shmakov, A. N.; Roger, A.-C.; Adamski, A. *Ni-loaded nanocrystalline ceria-zirconia solid solutions prepared via modified Pechini route as stable to coking catalysts of CH₄ dry reforming*. *Open Chem.* **2016**, 14, 363.
28. Priya, N. S.; Somayaji, C.; Kanagaraj, S. *Optimization of Ceria-Zirconia Solid Solution based on OSC Measurement by Cyclic Heating Process*. *Procedia Eng.* **2013**, 64, 1235-1241.
29. Djinović, P.; Črnivec, I. G. O.; Erjavec, B.; Pintar, A. *Details Behind the Self-Regeneration of Supported NiCo/Ce_{0.8}Zr_{0.2}O₂ Bimetallic Catalyst in the CH₄–CO₂ Reforming Reaction*. *ChemCatChem* **2014**, 6, 1652-1663.
30. Li, H.; Zhu, Q.; Li, Y.; Gong, M.; Chen, Y.; Wang, J.; Chen, Y. *Effects of ceria/zirconia ratio on properties of mixed CeO₂-ZrO₂-Al₂O₃ compound*. *J. Rare Earths* **2010**, 28, 79-83.
31. Gateshki, M.; Niederberger, M.; Deshpande, A. S.; Ren, Y.; Petkov, V. *Atomic-scale structure of nanocrystalline CeO₂–ZrO₂ oxides by total x-ray diffraction and pair distribution function analysis*. *J. Phys.: Condens. Matter* **2007**, 19, 156205.
32. Pakhare, D.; Spivey, J. *A review of dry (CO₂) reforming of methane over noble metal catalysts*. *Chem. Soc. Rev.* **2014**, 43, 7813-7837.

33. Caravella, A.; Brunetti, A.; Grandinetti, M.; Barbieri, G. *Dry Reforming of Methane in a Pd-Ag Membrane Reactor: Thermodynamic and Experimental Analysis*. *ChemEngineering* **2018**, *2*, 48.
34. Khairudin, N. F.; Sukri, M. F. F.; Khavarian, M.; Mohamed, A. R. *Understanding the performance and mechanism of Mg-containing oxides as support catalysts in the thermal dry reforming of methane*. *Beilstein J. Nanotechnol.* **2018**, *9*, 1162-1183.
35. Pakhare, D.; Spivey, J. *A review of dry (CO₂) reforming of methane over noble metal catalysts*. *Chem. Soc. Rev.* **2014**, *43*, 7813-7837.
36. Arora, S.; Prasad, R. *An overview on dry reforming of methane: strategies to reduce carbonaceous deactivation of catalysts*. *RSC Adv.* **2016**, *6*, 108668-108688.
37. Usman, M.; Wan Daud, W. M. A.; Abbas, H. F. *Dry reforming of methane: Influence of process parameters—A review*. *Renew. Sust. Energ. Rev.* **2015**, *45*, 710-744.
38. Mogensen, M.; Sammes, N. M.; Tompsett, G. A. *Physical, chemical and electrochemical properties of pure and doped ceria*. *Solid State Ionics* **2000**, *129*, 63-94.
39. Marrocchelli, D.; Bishop, S. R.; Tuller, H. L.; Yildiz, B. *Understanding Chemical Expansion in Non - Stoichiometric Oxides: Ceria and Zirconia Case Studies*. *Adv. Funct. Mater.* **2012**, *22*, 1958-1965.
40. Barsoum, M.; Barsoum, M. *Fundamentals of ceramics*. CRC press: 2002.
41. Rafique, A.; Raza, R.; Arifin, N. A.; Ullah, M. K.; Ali, A.; Steinberger-Wilckens, R. *Electrochemical and thermal characterization of doped ceria electrolyte with lanthanum and zirconium*. *Ceram. Int.* **2018**, *44*, 6493-6499.
42. Laachir, A.; Perrichon, V.; Badri, A.; Lamotte, J.; Catherine, E.; Lavalley, J. C.; El Fallah, J.; Hilaire, L.; Le Normand, F.; Quéméré, E.; Sauvion, G. N.; Touret, O. *Reduction of CeO₂ by hydrogen. Magnetic susceptibility and Fourier-transform infrared, ultraviolet and X-ray photoelectron spectroscopy measurements*. *J. Chem. Soc., Faraday Trans.* **1991**, *87*, 1601-1609.
43. López, J. M.; Gilbank, A. L.; García, T.; Solsona, B.; Agouram, S.; Torrente-Murciano, L. *The prevalence of surface oxygen vacancies over the mobility of bulk oxygen in nanostructured ceria for the total toluene oxidation*. *Appl. Catal., B* **2015**, *174*, 403-412.
44. Beale, A. M.; Weckhuysen, B. M. *EXAFS as a tool to interrogate the size and shape of mono and bimetallic catalyst nanoparticles*. *PCCP* **2010**, *12*, 5562-5574.
45. Hong, S. J.; Virkar, A. V. *Lattice Parameters and Densities of Rare-Earth Oxide Doped Ceria Electrolytes*. *J. Am. Ceram. Soc.* **1995**, *78*, 433-439.
46. Derafa, W.; Paloukis, F.; Mewafy, B.; Baaziz, W.; Ersen, O.; Petit, C.; Corbel, G.; Zafeiratos, S. *Synthesis and characterization of nickel-doped ceria nanoparticles with improved surface reducibility*. *RSC Adv.* **2018**, *8*, 40712-40719.
47. Zhou, Y.; Zhou, J. *Interactions of Ni Nanoparticles with Reducible CeO₂(111) Thin Films*. *J. Phys. Chem. C* **2012**, *116*, 9544-9549.
48. Senanayake, S. D.; Evans, J.; Agnoli, S.; Barrio, L.; Chen, T.-L.; Hrbek, J.; Rodriguez, J. A. *Water-Gas Shift and CO Methanation Reactions over Ni-CeO₂(111) Catalysts*. *Top. Catal.* **2011**, *54*, 34-41.
49. Barrio, L.; Kubacka, A.; Zhou, G.; Estrella, M.; Martínez-Arias, A.; Hanson, J. C.; Fernández-García, M.; Rodriguez, J. A. *Unusual Physical and Chemical Properties of Ni in Ce_{1-x}Ni_xO_{2-y} Oxides: Structural Characterization and Catalytic Activity for the Water Gas Shift Reaction*. *J. Phys. Chem. C* **2010**, *114*, 12689-12697.
50. Wang, R.; Fang, M. *Improved low-temperature reducibility in ceria zirconia nanoparticles by redox treatment*. *J. Mater. Chem.* **2012**, *22*, 1770-1773.
51. Aribi, K.; Soltani, Z.; Ghelamallah, M.; Granger, P. *Structure, morphology and reducibility of ceria-doped zirconia*. *J. Mol. Struct.* **2018**, *1156*, 369-376.
52. Zhang, F.; Liu, Z.; Zhang, S.; Akter, N.; Palomino, R. M.; Vovchok, D.; Orozco, I.; Salazar, D.; Rodriguez, J. A.; Llorca, J.; Lee, J.; Kim, D.; Xu, W.; Frenkel, A. I.; Li, Y.; Kim, T.; Senanayake, S. D. *In Situ*

Elucidation of the Active State of Co–CeO_x Catalysts in the Dry Reforming of Methane: The Important Role of the Reducible Oxide Support and Interactions with Cobalt. *ACS.Catal.* **2018**, 8, 3550-3560.

53. Zhou, X.-D.; Huebner, W. *Size-induced lattice relaxation in CeO₂ nanoparticles.* *Appl. Phys. Lett.* **2001**, 79, 3512-3514.

54. Deshpande, S.; Patil, S.; Kuchibhatla, S. V.; Seal, S. *Size dependency variation in lattice parameter and valency states in nanocrystalline cerium oxide.* *Appl. Phys. Lett.* **2005**, 87, 133113.

55. Rodriguez, J. A.; Grinter, D. C.; Liu, Z.; Palomino, R. M.; Senanayake, S. D. *Ceria-based model catalysts: fundamental studies on the importance of the metal–ceria interface in CO oxidation, the water–gas shift, CO₂ hydrogenation, and methane and alcohol reforming.* *Chem. Soc. Rev.* **2017**, 46, 1824-1841.

56. Smirnova, M. Y.; Bobin, A. S.; Pavlova, S. N.; Ishchenko, A. V.; Selivanova, A. V.; Kaichev, V. V.; Cherepanova, S. V.; Krieger, T. A.; Arapova, M. V.; Roger, A.-C.; Adamski, A.; Sadykov, V. A. *Methane dry reforming over Ni catalysts supported on Ce–Zr oxides prepared by a route involving supercritical fluids.* *Open Chem.* **2017**, 15, 412.

57. Simonov, M. N.; Rogov, V. A.; Smirnova, M. Y.; Sadykov, V. A. *Pulse Microcalorimetry Study of Methane Dry Reforming Reaction on Ni/Ceria-Zirconia Catalyst.* *Catalysts* **2017**, 7, 268.

TOC

